This is the accepted manuscript made available via CHORUS. The article has been published as:

# Low energy measurements of the $^{10}B(p,\alpha)^{7}Be$ reaction

M. Wiescher, R. J. deBoer, J. Görres, and R. E. Azuma

Phys. Rev. C **95**, 044617 — Published 26 April 2017

DOI: 10.1103/PhysRevC.95.044617

# Low energy measurements of the $^{10}$B$(p,\alpha)^7$Be reaction

M. Wiescher,[*] R. J. deBoer, and J. Görres

*Department of Physics, University of Notre Dame, Notre Dame IN, 46556*

R.E. Azuma

*Department of Physics, University of Toronto, Toronto, Canada M5S 1A7*
(Dated: April 9, 2017)

**Background:** The $^{11}$B$(p,2\alpha)^4$He reaction is being discussed as a prime candidate for advanced aneutronic fusion fuel systems. Particular interest in this reaction has recently emerged for laser driven plasma systems for energy generation and jet-propulsion systems. The lack of long-lived radioactive reaction products has been suggested as the main advantage of proton-boron fusion fuel. However, 19% of natural boron is $^{10}$B, with the $^{10}$B$(p,\alpha)^7$Be fusion reaction producing long-lived $^7$Be as a side product.

**Purpose:** A detailed measurement of the $^{10}$B$(p,\alpha)^7$Be reaction over the critical energy range of hot fusion plasma environments will help to determine the amount of $^7$Be radioactivity being produced. This information can be used in turn to monitor the actual fusion temperature by off-line measurement of the extracted $^7$Be activity. The goal of the here presented experiment is to expand on the results of earlier experiments, covering a wider energy range of interest for aneutronic plasma fusion applications, including also both $^{10}$B$(p,\alpha_0)^7$Be and the $^{10}$B$(p,\alpha_1)^7$Be reaction channels.

**Method:** The reaction cross section was measured over a wide energy range from $E_p = 400$ to 1000 keV using particle detection and from $E_p = 80$ to 1440 keV using $\gamma$-ray spectroscopic techniques. Reaction $\alpha$ particles were measured at different angles to obtain angular distribution information. The results are discussed in terms of an $R$-matrix analysis.

**Results:** The cross section data cover a wider energy range than previously investigated and bridge a gap in the previously available data sets. The cross sections show good agreement with previous results in the low energy region and show that the $^{10}$B$(p,\alpha_0)^7$Be channel is considerably larger than that of the $^{10}$B$(p,\alpha_1)^7$Be channel up to $E_p \approx 1$ MeV.

**Conclusions:** The new reaction data provides important new information about the reaction cross section over the entire energy range of plasma fusion facilities. This data, when coupled with previous measurement of the competing $^{10}$B$(p,\gamma)^{11}$C reaction will provide the opportunity for an extensive $R$-matrix analysis of the rather complex level structure in the $^{11}$C compound nucleus system.

## I. INTRODUCTION

Aneutronic plasma fusion systems have been increasingly discussed as possible energy sources without the disadvantage of long-lived radioactive end-products [1]. The most frequently quoted aneutronic energy sources are the $^3$He$(^3$He$,2p)^4$He ($Q$=12.9 MeV) and the $^{11}$B$(p,2\alpha)^4$He ($Q$=8.7 MeV) reactions. Of particular interest is the $^{11}$B$(p,2\alpha)^4$He reaction [2], which produces stable helium as the primary end-product and generates a sufficient amount of energy. This reaction has two primary advantages over the $^3$He$(^3$He$,2p)^4$He reaction. First, it does not require $^3$He, which is mostly produced as a decay product of tritium $^3$H [3, 4] and second, $^{11}$B is a naturally abundant and inexpensive fuel stock.

While the $^{11}$B+$p$ fusion system has already been considered as a potential energy source in traditional plasma systems [5–7] and for colliding beam reactors [8], recent observations of aneutronic fusion reactions on laser picosecond plasmas [9] have motivated the discussion of other possible applications. One such application uses the $^{11}$B$(p,2\alpha)^4$He reaction for laser driven hot pulsed

plasma systems [10–12], and another proposes laser jet propulsion systems for long distant space travel [13]. The optimal energy range for a $^{11}$B+$p$ fusion system is between $E_{c.m.} = 200$ and 1000 keV. This is because a broad resonance structure has been observed at $E_{c.m.} \approx 600$ keV [14] that dominates the total cross section of the reaction. Therefore the efforts of laser driven fusion studies focus on that energy range [15].

While the $^{11}$B$(p,2\alpha)^4$He fusion reaction does not produce any long-lived radioactive products, the 19% $^{10}$B abundance in naturally occurring boron fuel material will produce the longer-lived $^7$Be isotope through the $^{10}$B$(p,\alpha)^7$Be reaction. $^7$Be decays by electron capture with a laboratory life-time of 53.3 days with a 10% transition to the first excited state in $^7$Li. The $^7$Li subsequently $\gamma$-decays to the ground state under emission of a characteristic 478 keV $\gamma$-line [16]. The total cross section of the reaction near $E_{c.m.} \approx 600$ keV is $\sigma_{total} \approx 10$ mb according to the EXFOR data compilation [17]. This is substantially lower than the 1 barn cross section reported for $^{11}$B$(p,2\alpha)^4$He reaction [14]. The production of a spurious amount of $^7$Be in a plasma fusion operation with enriched $^{11}$B fuel may therefore not be a matter of great concern, but the observation of $^7$Be from a boron-hydrogen plasma burning environment, doped with a well know amount of $^{10}$B may provide the means for tempera-

* Michael.C.Wiescher.1@nd.edu

ture determination in the plasma region. This may serve as an independent test for temperature analysis in the new generation of laser driven hot plasma facilities such as the National Ignition Facility [18], were recent studies of $d-t$ and $d-d$ fusion signals indicated considerable uncertainty in the temperature analysis [19].

Yet, the EXFOR data [17], shown in Fig. 1, indicate significant differences and uncertainties between the different experimental data sets for the possible transitions to the ground state $^{10}$B$(p,\alpha_0)^7$Be and the first excited state $^{10}$B$(p,\alpha_1)^7$Be in $^7$Be. The ground state transition has been measured extensively in the low energy range between 100 keV and 1 MeV [20–29], with some experiments covering a higher energy range as well [30–32]. These results already show noticeable deviations from one another as displayed in Fig. 1. The $^{10}$B$(p,\alpha_1)^7$Be reaction has seen significantly less study and there is a wide gap in the experimental measurements between the low energy data of Angulo *et al.* [33] and the higher energy measurements [31, 34–41]. Complicating the interpretation of the data, the level structure in this region, just above the proton separation energy in $^{11}$C, is characterized by a number of unbound states as indicated in Fig. 2. However, the detailed way these levels contribute as broad overlapping and possibly interfering resonances to the reaction cross section is not well understood. Additionally, several data sets have been measured using the activation technique [42–44]. These data then represent the total $^{10}$B$(p,\alpha)^7$Be cross section (i.e. the sum of the $^{10}$B$(p,\alpha_0)^7$Be and $^{10}$B$(p,\alpha_1)^7$Be cross sections at these low energies).

As noted previously [47], in the low energy range the data of Bach and Livesey [22] exhibit a pronounced difference to other data sets. This can most likely be explained by a deviation of 10 to 15 keV in the energy calibration of their experiment. This seems large by modern standards, but the energy calibration used at the time (1955) was based only on voltage readings and not on a direct measurement of the beam energy. Other discrepancies can be observed at energies above 1 MeV, in particular between the data of Kalinin *et al.* [42] and those of Kafkarkou *et al.* [45]. The cross section values given by the earlier measurement [42] are based on the activation technique where the authors measured the characteristic decay activity of $^7$Be. These results also indicate considerably larger values than the later work of Kafkarkou *et al.* [45], which is based on the direct measurement of the emitted $\alpha$ particles. Kalinin *et al.* [42] used targets that were more than an order of magnitude thicker than the transmission targets used by Kafkarkou *et al.* [45]. The difference, therefore, might be due to target integration effects that were not fully corrected in the earlier work. Indeed, when the thick target data of Roughton *et al.* [43] (not shown) were unfolded for generating cross sections [47], they were found to be in good agreement with other data, albeit with large uncertainties as shown in the bottom panel of Fig. 1.

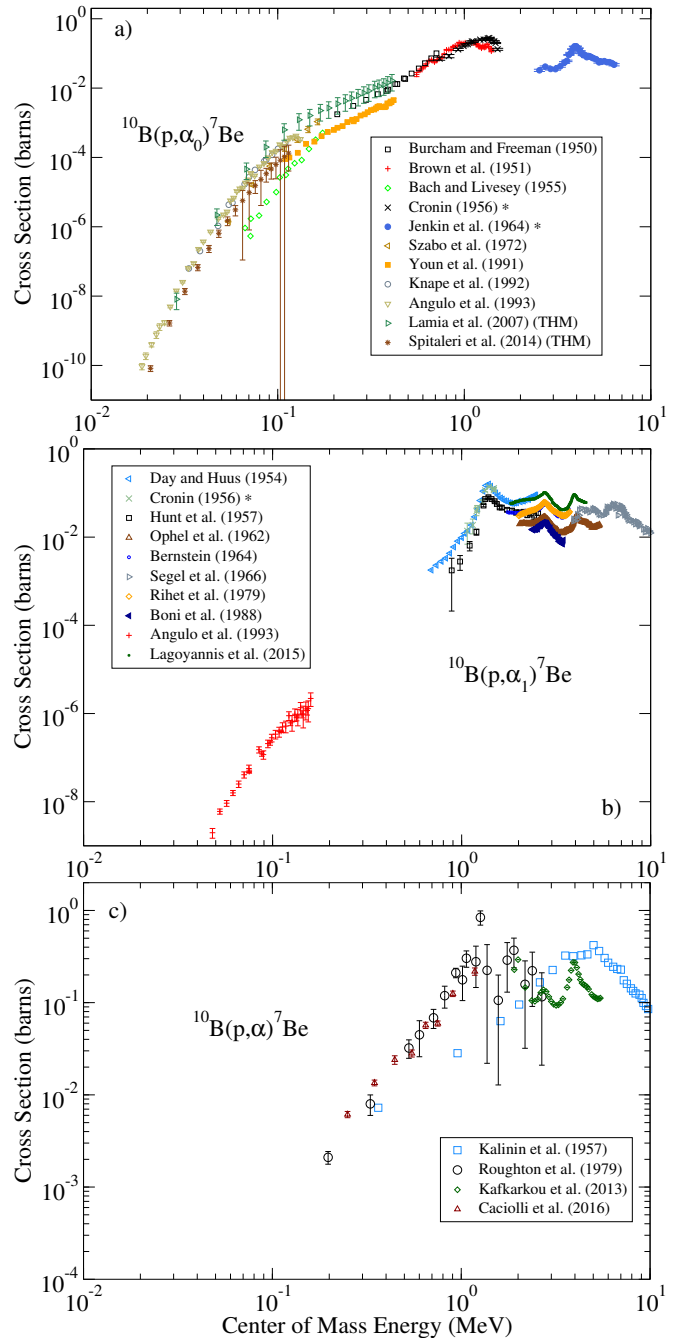Low energy data have relied on the direct measure-



FIG. 1. (Color online) Cross section data for the reaction $^{10}$B$(p,\alpha)^7$Be, based on 64 years of experimental work and compiled in the EXFOR data base [17]. Data are in their raw form, not subjected to any later re-normalization recommendations. The top part of the figure (a) shows cross sections determined by prompt detection of $\alpha$ particles to the ground state, the middle part (b) shows measurements of the cross section to the first excited state, and the lower (c) are those determined by the activation method (total $(p,\alpha)$ cross sections). The exception is that of Kafkarkou *et al.* [45] where both the $\alpha_0$ and $\alpha_1$ particles were detected directly but only the sum of the cross sections is reported. Note that because of the lack of higher energy angle integrated cross section data, some differential data have been scaled by $4\pi$ to facilitate the comparison. They are indicated by an $*$ sign.

$E_x$ (MeV)    $J^\pi$

12.27  12.65  12.51                    $1/2^-$  $(7/2^+)$ $(^{10}B + p_4)$ $(^8Be + {}^3He_1)$
12.25  12.40                            ???
12.11  12.16                            ???  $(^7Be + \alpha_2)$

11.44                                   ???
10.84  11.03                            ???
10.43  10.68                            $9/2^\pm$  $(^{10}B + p_3)$
       10.08                            $7/2^-$ $(7/2)$ $(^{10}B + p_2)$
9.97   9.78                             $(5/2)^-$ $(3/2)$ $^{10}B$
9.65                                    $5/2^-$ $(^{10}B + p_1)$
9.41   9.20                             $8Be + {}^3He$
9.22
$^{10}B + p$  8.69  8.65  8.70  $5/2^+$  $7/2^+$ $^{10}B + p$
       8.42                             $5/2^-$
7.97   8.10                             $3/2^-$
$^7Be + \alpha$  7.54  7.50             $3/2^\pm$  $^7Be + \alpha$  $^7Be + \alpha_1$

6.90                                    $5/2^+$
6.34   6.48                             $7/2^-$ $1/2^+$

4.80                                    $3/2^-$
4.32                                    $5/2^-$

2.00                                    $1/2^-$

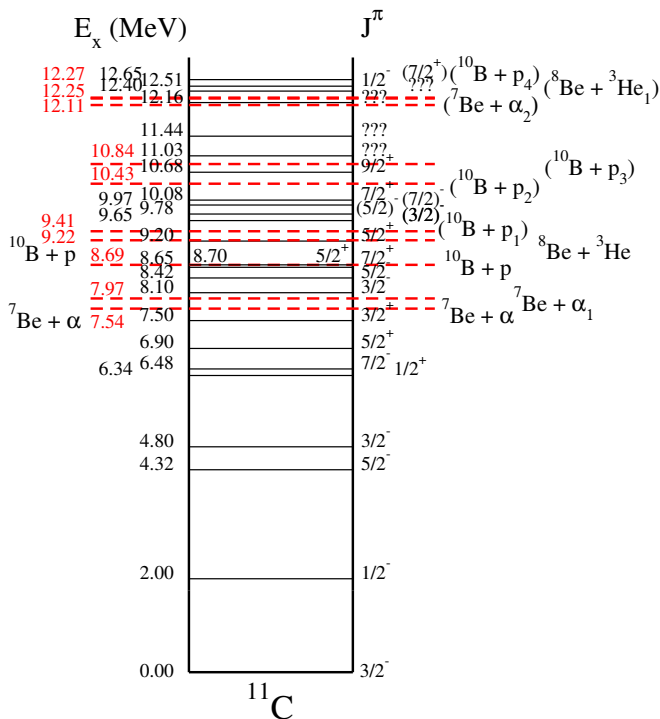0.00                                    $3/2^-$

$^{11}C$

FIG. 2. (Color online) Level diagram of the $^{11}C$ compound nucleus [46]. The red dashed lines indicate different particle separation energies. The nucleus becomes $\alpha$ unbound at $S_\alpha = 7.54$ MeV and then proton unbound at $S_p = 8.69$ MeV. The level density begins to increase rapidly above the proton separation energy and the levels are characterized by large particle widths of the order hundreds of keV. This has made disentangling the level structure quite challenging. Above $E_x = 11$ MeV the level properties become highly uncertain.

ments of the reaction cross section by Angulo *et al.* [26, 33]. Based on these results it was suggested that the data by Youn *et al.* [24], that stretch to a somewhat higher energy, should be corrected by a factor 1.83. In a recent experiment by Spitaleri *et al.* [29] the Trojan Horse Method (THM) has been applied to the quasifree $^2H(^{10}B, \alpha_0)^7Be$ reaction at a boron-beam energy of 24.5 MeV (preliminary measurements reported in [27, 28, 48]).[1] The THM analysis of the experimental data leads to the determination of the $^{10}B(p, \alpha_0)^7Be$ cross section at low energy, but it must be matched to previous results at higher energies to obtain the absolute scale. An $R$-matrix prediction was also made based on the level parameters available in the literature. It shows a peculiar energy dependence in the energy range between 0.5 and 1.0 MeV, where it under-produces the

experimental data [20, 30, 31]. This has been interpreted as an indication for the existence of a possible resonance state in that excitation range that was not included in the $R$-matrix parameter set. Such a resonance structure has already been suggested by the $^{10}B(p, \gamma)^{11}C$ radiative capture study, which indicated the existence of several strong broad and interfering resonance states in this excitation range [50]. An alternative explanation could be non-resonant direct reaction contributions that could be described in the framework of a 3-particle transfer reaction model [51] or the low energy tail of a very broad resonance(s) at higher energies.

A recent study by Caciolli *et al.* [44] attempted to address this issue by measuring the total cross section of the $^{10}B(p, \alpha)^7Be$ reaction at energies between $E_{c.m.} = 250$ and 1200 keV. The experiment was based on the activation technique, measuring the 478 keV $\gamma$-ray activity of the $^7Be$ reaction products at eight different irradiation energies. The data are a factor of two higher than the data of in the previous work by Youn *et al.* [24], which seems to confirm the former assessment by Angulo *et al.* [26] that the latter data need to be modified by a factor 1.83.

Another recent measurement by Lombardo *et al.* [52] observed ground state $\alpha$ particles over the range from $E_p = 600$ to 1000 keV. The kinematics at these energies result in very similar energies for the scattered protons and reaction $\alpha$ particles, complicating the separation of the individual cross sections. This experiment used an inverse absorber technique to determine the individual yields at several angles relative to the beam. This technique utilizes detectors placed at mirror angles to the beam axis. One set of detectors is masked by a thin foil whose thickness is tuned so that protons can penetrate the foil but $\alpha$ particles are stopped. After correcting for the effects of the absorber foil on the energies of the particles, a subtraction of the two spectra can be made to separate out the yields from the protons and $\alpha$ particles.

In addition to the experimental work, the authors performed the first multichannel $R$-matrix fit to a subset of $^{10}B(p, \alpha_0)^7Be$, $^{10}B(p, \alpha_1)^7Be$, and $^{10}B(p, p)^{10}B$ data from the literature. The fit was made over the excitation energy range from 9.2 to 11.0 MeV (500 to 2300 keV center-of-mass energy), covering the range where the $^{10}B(p, \alpha_1)^7Be$ cross section begins to compete with that of the $^{10}B(p, \alpha_0)^7Be$. A consistent fit was obtained but an additional state at $E_x = 9.36$ MeV of $J^\pi = 5/2^-$ was required. The fit also highlights the rather poor state of the data over this energy region. Much of the data have large uncertainties and the authors needed to assume isotropy for some of the higher energy differential cross section data in order to generate a complete set of angle integrated data covering the entire energy range.

Before using the $^{10}B(p, \alpha)^7Be$ reaction as a reliable monitor for plasma fusion conditions, the present inconsistencies in the experimental data need to be removed and a reliable interpretation of the reaction mechanism needs to be obtained over the entire low energy

---

[1] During the submission of this work, Spitaleri *et al.* [49] has published an extended THM measurement, which covers an energy range up to $E_{c.m.} = 1.5$ MeV. At low energies the measurements are in general agreement with previous work, but the effect of the new higher energy data on the $R$-matrix fit has not yet been determined.

range. This requires more detailed cross section measurements for the two open reaction channels at low energies: $^{10}$B$(p,\alpha_0)^7$Be and $^{10}$B$(p,\alpha_1)^7$Be. Transitions to higher-lying final states do not become energetically allowed until higher energies as shown in Fig. 2. The cross section measurements need to be complemented by angular distribution studies to identify the nature of the reaction mechanism. These are most likely contributions from broad resonance states in the $^{10}$B$(p,\alpha)^7$Be reactions. The reaction channels that feed higher excited states in $^7$Be open at higher energies, above $E_p = 3.2$ MeV (e.g. $S_{a_2} = 12.11$ MeV, $E_p = 3.77$ MeV, see Fig. 2). The $^{10}$B$(p,{}^3$He$)^7$Be threshold is at $E_p = 590$ keV but the lowest energy measurements do not begin until $E_p \approx 4.0$ MeV [53]. However, penetrability arguments, and the lack of experimentally observed lower energy yields, suggest this reaction remains weak up to these higher energies. Additionally, inelastic proton scattering, $^{10}$B$(p,p_1)^{10}$B can occur at energies above $E_p \approx 790$ keV. This cross section has been measured down to $E_p \approx 1.5$ MeV by Day and Huus [34] but remains weak until $E_p \approx 2.5$ MeV [36, 41]. Both of these reaction channels should be further investigated at low energies. An additional direct 3-particle transfer component that is energetically possible above $E_p \approx 490$ keV. These additional channels are assumed to make a negligible contribution to the total cross section at energies below $E_p = 3$ MeV.

For these purposes, we have performed an independent study of the $^{10}$B$(p,\alpha)^7$Be reaction. We investigated both the $\alpha_0$ (0.4 to 1 MeV proton energy) as well as the $\alpha_1$ (0.08 to 1.44 MeV proton beam energy) channels to the ground state and the first excited state in $^7$Be, respectively, using particle and $\gamma$ spectroscopy methods. Also measured were the angular distributions in the $^{10}$B$(p,\alpha_0)^7$Be channel to investigate possible deviations from the isotropic distribution reported in earlier work [26]. Such deviations would indicate a change in reaction mechanism or signal interference effects between different resonance components. In the following section we describe the experimental set-up and provide a description of the data and cross section analysis. This will be complemented by an $R$-matrix analysis that includes data from several past measurements for the reactions $^{10}$B$(p,p_0)^{10}$B, $^{10}$B$(p,\alpha_0)^7$Be and $^{10}$B$(p,\alpha_1)^7$Be. This approach may help to reduce the overall uncertainties, as most previous $R$-matrix analyses of the $^{11}$C compound system were based on only a single channel.

## II. EXPERIMENTAL SET-UP AND ANALYSIS

The experiment was performed at the JN accelerator of the University of Toronto, now located at the Nuclear Science Laboratory of the University of Notre Dame. The machine provided proton beam currents of up to 30 $n$A on enriched $^{10}$B transmission targets and up to 70 $\mu$A on water cooled beam-stop targets during the course of the experiment. For the $^{10}$B$(p,\alpha)^7$Be particle spectroscopy experiments, the targets were prepared by evaporating a thin layer of 20 $\mu$g/cm$^2$ 93% enriched $^{10}$B onto a 10 $\mu$g/cm$^2$ thin carbon foil forming an amorphous BC layer. For the $^{10}$B$(p,\alpha_1 - \gamma)^7$Be measurements, the targets were mounted as beam-stop targets with a thin layer of 55 $\mu$g/cm$^2$ enriched $^{10}$B (93%) evaporated onto a clean 0.3 mm thick Ta-backing.

For measuring the $\alpha$ particles, four Si surface barrier detectors were mounted around the transmission target in a scattering chamber. The target had an orientation of 130° with respect to the beam direction and the detectors were mounted at angles of 45, 60, 90 and 120° with respect to the beam axis. During the runs, the reaction induced $\alpha$ particles, as well as the protons from elastic scattering, were recorded. Since BC targets oxidize easily [54], elastic proton scattering on $^{16}$O was also measured and was recorded for beam normalization.

The reaction data obtained from particle detection were normalized to elastic $^{10}$B$(p,p)^{10}$B scattering data at $E_p = 400$ keV. It will be demonstrated later that the low energy $^{10}$B$(p,p)^{10}$B data of Chiari $et$ $al.$ [55] deviate from Rutherford scattering at energies as low as $E_p = 500$ keV. However, the same $R$-matrix calculations that well describe that data give a maximum deviation of 5% at $E_p = 400$ keV (at 180°). At 120°, the largest observation angle in the present measurements, the deviation just exceeds 3% at $E_p = 400$ keV. Therefore a conservative estimate of 5% systematic uncertainty is recommended for the particle detection measurements. This systematic uncertainty should be considered independent for each angle. Additionally, the measured $^{10}$B$(p,\alpha)^7$Be reaction yield showed no pronounced narrow resonance structures in the investigated energy range and the thin target yield formalism [56] was utilized to determine the cross section.

For measuring the yield of the 429 keV radiation from the $^{10}$B$(p,\alpha_1-\gamma)^7$Be reaction, the solid beam-stop target was mounted at 55° with respect to the beam direction and a Ge detector with 35% relative efficiency was set-up in close geometry facing the target backing. The detection efficiency was determined with calibrated $^{56}$Co and $^{60}$Co sources. In addition, the efficiency was determined with respect to the well-known non-resonant cross section of the $^{16}$O$(p,\gamma)^{17}$F reaction [57] and the strength of the $^{27}$Al$(p,\gamma)$ resonance at 632 keV [58]. A liquid nitrogen cooled copper shroud was mounted in front of the target to reduce carbon deposition. The shroud together with the target formed a Faraday cup for charge determination. The measured yield was normalized to the collected charge during each run. For a detailed description of the arrangement see [50].

The cross section excitation curve for the $^{10}$B$(p,\alpha_0)^7$Be ground state transition was determined for all four detection angles over the laboratory proton energy range from 400 to 1000 keV. The reaction channel to the first excited state in $^7$Be, $^{10}$B$(p,\alpha_1)^7$Be, could not be recorded because it could not be separated from the
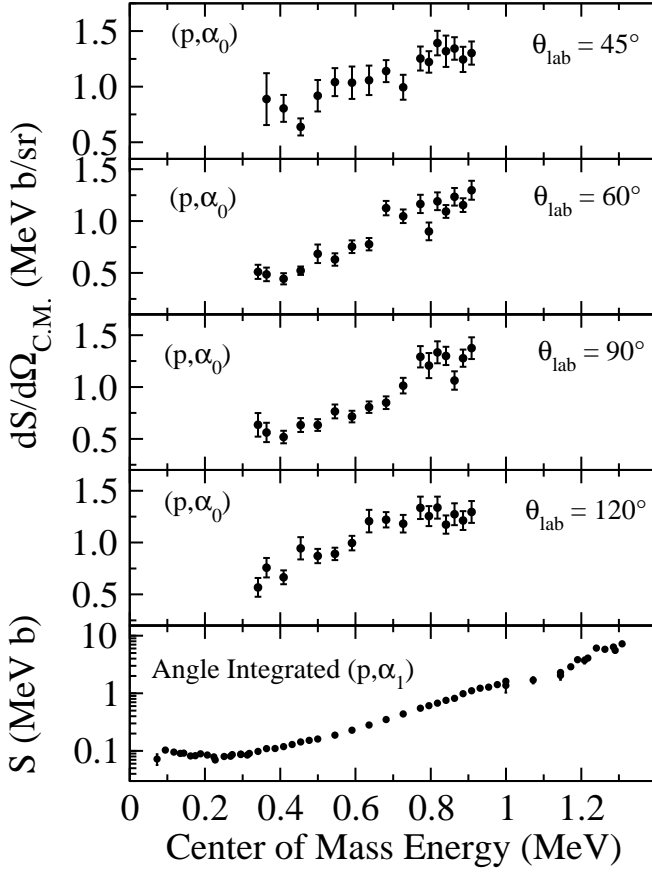
FIG. 3. (Color online) Differential $S$-factor excitation curves for the $^{10}\mathrm{B}(p,\alpha_0)^7\mathrm{Be}$ transition taken at four angles (lab) and total $S$-factor excitation curves for the $^{10}\mathrm{B}(p,\alpha_0)^7\mathrm{Be}$ ground state and the $^{10}\mathrm{B}(p,\alpha_1)^7\mathrm{Be}$ first excited state transitions in $^7\mathrm{Be}$ based on the present data set. In the lower energy range, near 400 keV, the ground-state transition is nearly two orders of magnitude stronger than the transition to the first excited state in $^7\mathrm{Be}$. The ratio of the cross section of the $^{10}\mathrm{B}(p,\alpha_1)^7\mathrm{Be}$ to $^{10}\mathrm{B}(p,\alpha_0)^7\mathrm{Be}$ reactions generally increases towards higher energies as shown in Fig. 5. At 900 keV, this ratio is about one order of magnitude.

strong elastic scattering $^{10}\mathrm{B}(p,p)^{10}\mathrm{B}$ and $^{12}\mathrm{C}(p,p)^{12}\mathrm{C}$ in the here investigated energy range. Further, the $^{10}\mathrm{B}(p,\alpha_1)^7\mathrm{Be}$ yields vary between 1 and 2 orders of magnitude weaker than those from $^{10}\mathrm{B}(p,\alpha_0)^7\mathrm{Be}$ over the experimentally investigated region. The cross sections for the ground state transitions have been converted to the astrophysical $S$-factor for better comparison with existing data. The astrophysical $S$-factor for the $^{10}\mathrm{B}+p$ system is defined as a function of the center-of mass energy in units (MeV) and the reaction cross section $\sigma(E)$ in units (barn):

$$S(E) = \sigma(E) \cdot E \cdot e^{(18.869 \cdot E^{-1/2})}. \qquad (1)$$

The resulting excitation curves for the differential $S$-factors of the $^{10}\mathrm{B}(p,\alpha_0)^7\mathrm{Be}$ reaction are shown in Fig. 3 together with the total $S$-factor extracted from these
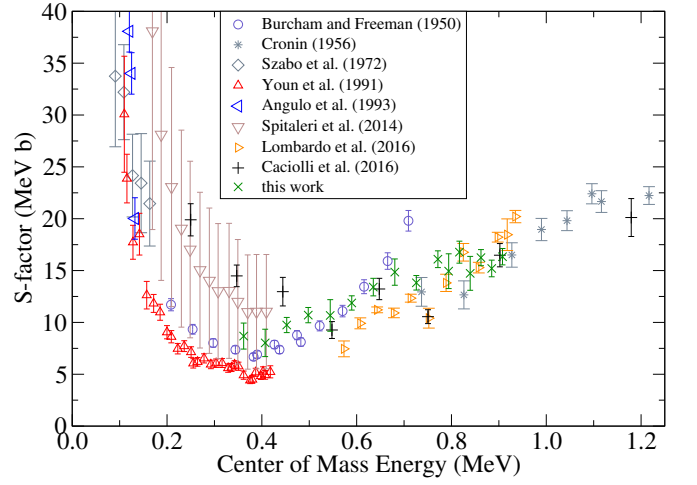


FIG. 4. (Color online) Total $S$-factor excitation curve for the $^{10}\mathrm{B}(p,\alpha_0)^7\mathrm{Be}$ transition in comparison with previous work. The data by Youn $et\ al.$ [24] are lower in the overlapping energy range, while the THM data by Spitaleri $et\ al.$ [29] are higher. However, the data of Spitaleri $et\ al.$ [29] are normalized to the direct measurements of Angulo $et\ al.$ [26] at substantially lower energies in the tail of the $E_{\mathrm{c.m.}} = 10(2)$ keV threshold resonance. The recent measurements by Caciolli $et\ al.$ [44], using activation techniques, agree in the higher energy range but deviate substantially at energies below 500 keV, matching the THM predictions.

data. Also shown is the $S$-factor excitation curve for the $^{10}\mathrm{B}(p,\alpha_1-\gamma)^7\mathrm{Be}$ 429 keV transition. Both $\alpha_0$ and $\alpha_1$ transitions appear fairly flat but lower energy data [26, 33] suggest a smooth increase in $S$-factor towards low energies. In the low energy range the strength of the $^{10}\mathrm{B}(p,\alpha_1-\gamma)^7\mathrm{Be}^*$ reaction channel is substantially weaker than the one for the ground state transition $^{10}\mathrm{B}(p,\alpha_0)^7\mathrm{Be}$. At 400 keV it represents only 1% of the total reaction cross section. However, the strength of the $^{10}\mathrm{B}(p,\alpha_1)^7\mathrm{Be}$ reaction increases more rapidly with energy and is about 10% of the total strength near 900 keV. At higher energies a comparable strength for both reaction channels has been observed in previous work [30]. Fig. 4 shows the $S$-factor of the $^{10}\mathrm{B}(p,\alpha_0)^7\mathrm{Be}$ reaction branch in comparison with previous results. This figure underlines the uncertainties that hamper the present data sets.

The here presented data set does not overlap with the data of Angulo $et\ al.$ [26], so a direct comparison is not possible. A direct comparison with the predictions by Spitaleri $et\ al.$ [29] are difficult, since these data are not absolute measurements but are normalized to the cross section data given in Ref. [26]. Within the given uncertainties they agree with the present data in the overlapping energy range. Similarly, the new $S$-factor data also agree well with the $S$-factor numbers quoted by Youn $et\ al.$ [24] (after being scaled by the factor of 1.83), albeit the increase in $S$-factor towards lower energies is not as obvious. This discrepancy is even more visible in
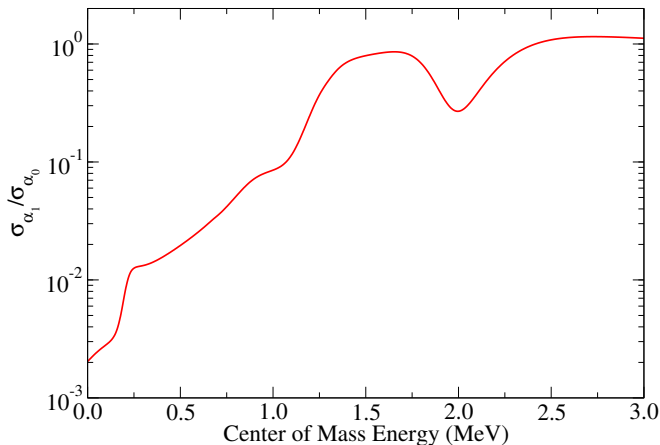
FIG. 5. (Color online) Ratio of the $^{10}$B$(p,\alpha_1)^7$Be cross section to that of $^{10}$B$(p,\alpha_0)^7$Be $\sigma_{\alpha_1}/\sigma_{\alpha_0}$. The $^{10}$B$(p,\alpha_1)^7$Be cross section is relatively small at low energy but increases rapidly, but becomes of similar strength above about $E_{\rm c.m.} \approx 1$ MeV.



FIG. 6. (Color online) The Legendre polynomial fit parameters $a_1$ (a) and $a_2$ (b) for the angular distribution are displayed as function of energy, indicating a deviation from isotropy between 400 and 700 keV. Besides the results of the present experiment, the figure also shows the angular distribution data of two previous studies [24, 31].

the comparison with the $S$-factor predictions by Caciolli *et al.* [44], which strongly deviate from the present results in the energy range below 500 keV. However, there is good agreement towards higher energies. This agreement can also be observed in comparison with the data by Cronin [31] below 800 keV.

One explanation for these energy dependent deviations can be possible contributions from the $^{10}$B$(p,\alpha_1)^7$Be reaction channel. Brown *et al.* [30] and Cronin [31] suggested a strong $\alpha_1$ contribution above 1.3 MeV, however, these measurements did not include the lower energy range and possible $\alpha_1$ resonance contributions to the total cross section cannot be excluded. Fig. 5 shows the ratio of the total $S$-factors of the $^{10}$B$(p,\alpha_1)^7$Be and the $^{10}$B$(p,\alpha_0)^7$Be channels based on the R-matrix fit discussed below. While displaying a small bump in the ratio around 500 keV it does not indicate a major contribution of the $^{10}$B$(p,\alpha_1)^7$Be channel to the total cross section.

A critical feature for determining and identifying the various reaction components are changes in the angular distribution of the emitted $\alpha$ particle as a function of energy. The angular distribution data obtained in this experiment were fit in terms of a Legendre polynomial function to compare the results with previous claims of anisotropies in this energy range [24]. The polynomial fit parameters $a_1$ and $a_2$ reflect the angular distribution dictated by the angular momenta associated with the reaction process. Fig. 6 shows the Legendre fit parameters as a function of energy normalized to the $a_0$ term, that describes the total cross section (as shown in Fig. 3). Also shown are the results of former work [24, 31]. The present data indicate isotropy for the energy range above 700 keV and below 350 keV as observed in previous work [31]. Deviation from an isotropic distribution is observed for the energy range between 400 keV and 700 keV. This presents itself as an increase in the $a_2$
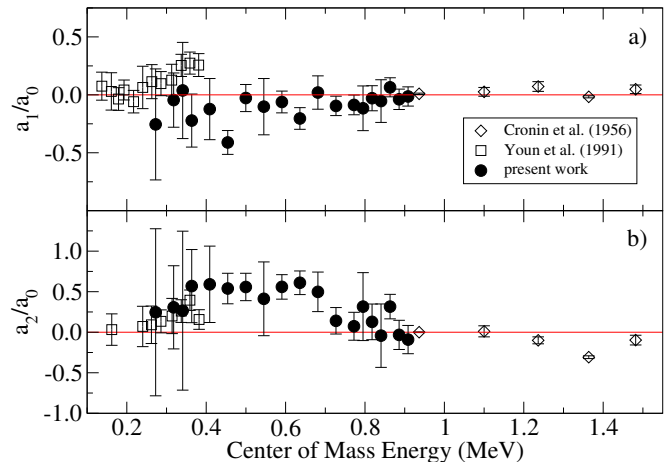
term. This is also reflected in the angular distribution data of [24]. However, their claim of an increasing $a_1$ term cannot be confirmed because of the uncertainty in the present data set. The energy range between 400 and 700 keV corresponds to the range for which the $R$-matrix calculation of [29] fails to reproduce the $S$-factor data of previous thick target measurements [43] (see Fig. 12 of that work). The anisotropy in the angular distribution data of the present thin target measurements provides additional evidence for a resonance contribution in this particular energy range as will be discussed in the following section.

## III. $R$-MATRIX ANALYSIS

$R$-matrix analyses have been made previously by several authors [44, 52, 59, 60] where the most comprehensive is the multi-channel analysis of Lombardo *et al.* [52]. While a good fit was obtained by Lombardo *et al.* [52], the analysis was limited to the proton energy range between 600 and 1000 keV, corresponding to an excitation energy range from $9.2 < E_x < 11.0$ MeV. In this work the fit is extended to include the lower energy data down to the proton separation energy ($S_p = 8.6894(9)$ MeV).

The present $R$-matrix analysis includes $^{10}$B+$p_0$, $^7$Be+$\alpha_0$, and $^7$Be+$\alpha_1$ particle pairs. This analysis is truncated at an upper energy limit of $E_x = 10.5$ MeV ($E_{\rm c.m.} = 1.8$ MeV). As discussed in Sec. I, while both $^{10}$B+$p_1$ and $^8$Be+$^3$He channels open in this energy range, previous measurements [34, 53] have shown that these cross sections remain small compared with the uncertainties on the data in the dominating channels, hence they are neglected. The capture channel, also small compared to the total reaction cross section, has been neglected but

will be considered in a forthcoming analysis. A channel radius of 5.0 fm was used for the proton channels, while 5.5 fm was used for the $\alpha$ channels. Variations in these radii were observed to not have a significant effect on the quality of the fit.

Table I summarizes the different data sets used for the $R$-matrix analysis. Whenever possible, primary data (i.e. data closest to the measured yields) have been utilized. Many older measurements lack tabulated cross sections but most have been digitized from the figures of those works by EXFOR [17].

A few of the data sets in the literature are found to be in poor agreement with the majority of previous results. The disagreements are not just ones of overall normalization, but are energy dependent as discussed in Sec. II. These data sets have been excluded from the $R$-matrix analysis. Additionally, the $^7$Be+$\alpha$ data have been neglected from the fit for reasons that will be discussed in Sec. III D.

It is especially important to include differential cross sections for the reactions under consideration because the resonances are often broad and overlapping, making them difficult to resolve in the total cross section. The additional interferences that occur in the differential cross sections add further constraints in deducing the level properties of the underlying compound nucleus states. However, at low energy, both the $(p, \alpha_0)$ and the $(p, \alpha_1)$ cross sections are nearly isotropic, making high precision measurements necessary to observe these effects. Angular distributions have been taken from Youn et al. [24], Cronin [31] and differential excitation curves from Brown et al. [30], Cronin [31], Jenkin et al. [32], Chiari et al. [55], Overley and Whaling [61] and this work.

## A. The Analysis of the $^{10}$B$(p, p)$ Scattering Data

Important additional information for the $R$-matrix analysis is provided by the study of $^{10}$B$(p, p_0)^{10}$B elastic scattering. There are three measurements of low energy proton elastic scattering on $^{10}$B, those of Brown et al. [30], Overley and Whaling [61], and Chiari et al. [55], but the measurement of Brown et al. [30] is at only one angle and covers a rather limited energy range. All the measurements appear to be in reasonable agreement, however the data of Overley and Whaling [61] do not provide detailed uncertainties. Two distinct resonances appear to dominate the cross section at $E_{c.m.} = 1.39$ and 1.99 MeV that correspond to the levels at $E_x = 10.08$ $(7/2^+)$ and 10.68 $(9/2^+)$ MeV. However, there are other broad states in this region like the $E_x = 10.10$ MeV $(5/2^+)$ state proposed by Lombardo et al. [52] and the $E_x = 9.98$ MeV $(7/2^-)$ state proposed by Wiescher et al. [50] that also make more subtle contributions to the cross section. Further, lower energy resonances are mostly masked by Coulomb scattering.

A fairly good reproduction of the scattering cross section can be obtained with the levels included in the $R$-

matrix fit as shown in Fig. 7. The fit is of similar quality to that given in Lombardo et al. [52] but has been expanded to include all the data of Brown et al. [30], Overley and Whaling [61], and Chiari et al. [55]. The data of Overley and Whaling [61] and Chiari et al. [55] are in excellent agreement. Those of Brown et al. [30] also match the shape of the other measurements, but are low in absolute normalization by about 20%. However, this is equivalent to the uncertainty in the digitization procedure quoted by EXFOR for this data.

A rare feature of the scattering data is that even at very low energy there is deviation from Coulomb scattering. Although, since it is slowly varying in energy, it seems that this has been overlooked previously. This may be responsible for some of the normalization issues observed in the different data sets. This is illustrated, for example, in Fig. 8 of Lombardo et al. [52] where the $R$-matrix fit under-produces the experimental data at the lowest energies. This deviation can be explained by the contribution from the $E_{c.m.} = 10(2)$ keV threshold resonance state at $E_x = 8.6987$ MeV. Including this level in the $R$-matrix gives a better match to the low energy cross section data as shown in Fig. 7. Because this resonance is strong, narrow, and isolated, this state provides a clear link between the scattering, $(p, \alpha_0)$, $(p, \alpha_1)$, and $(p, \gamma)$ cross sections at low energy where this state dominates. Because the partial widths of this prominent resonance are known, this provides a constraint on the absolute scale of the scattering data. $\Gamma_p \approx 2 \times 10^{-14}$ eV has been determined recently from the THM measurements of Spitaleri et al. [29] and the $\alpha$ width ($\Gamma_{\text{total}} \approx \Gamma_{\alpha_0}$) has been measured by Fortune et al. [62] as $\Gamma_{\alpha_0} = 15(1)$ keV. This is a valuable cross check between these different reaction channels since the boron target thickness are difficult to determine experimentally because no narrow resonances exist in the proton induced cross sections.

## B. The Analysis of the $^{10}$B(p,$\alpha$) Cross Section Data

The majority of the data in the literature focus on the $^{10}$B$(p, \alpha_0)^7$Be cross section as it is the largest reaction cross section at low energy. Much of this low energy data is in reasonable agreement as far as their absolute scale is concerned apart from the data of Youn et al. [24]. This data has to be scaled up, and Angulo et al. [26] has suggested a factor of 1.83. However, there are random variations in the point-to-point cross section data of several measurements that are significantly larger than the uncertainties suggest are reasonable. This is especially true for the low energy data of Angulo et al. [26].

At higher energy, the majority of the data are also in reasonable agreement as far as their absolute scales are concerned. The exception here are the data of Jenkin et al. [32]. In the current analysis it has been observed that these data need to be scaled up by a factor of 2 to match the other data sets. Their energy dependence is then in good agreement with the other data. In the

TABLE I. Summery of experimental data. A significant amount of data was obtained by digitization of figures from the original works and made available by EXFOR [17]. The data considered in the $R$-matrix fit are labeled "Fitted Data". Data found to be inconsistent with the majority are labeled "Inconsistent Data". A consistent fit could also not be obtained with the current $^7$Be + $\alpha$ data.

| Ref. | Reaction(s) | Source |
|---|---|---|
| **Fitted Data** | | |
| Burcham and Freeman [20] (1949) | $^{10}$B$(p, \alpha_0)^7$Be | Fig. 11 (EXFOR) |
| Burcham and Freeman [21] (1950) | $^{10}$B$(p, \alpha_0)^7$Be | Fig. 7 (EXFOR) |
| Brown $et\ al.$ [30] (1951) | $^{10}$B$(p, p)^{10}$B | Fig. 9 (EXFOR) |
| Cronin [31] (1956) | $^{10}$B$(p, \alpha_{0,1})^7$Be | Fig. 5 (EXFOR) |
| Overley and Whaling [61] (1962) | $^{10}$B$(p, p)^{10}$B | Figs. 2 and 3 (EXFOR) |
| Jenkin $et\ al.$ [32] (1964) | $^{10}$B$(p, \alpha_{0,1})^7$Be | Figs. 2, 3, and 4 (EXFOR)[a] |
| Roughton $et\ al.$ [43] (1979) | $^{10}$B$(p, \alpha_{\text{total}})^7$Be | Table 2[b] |
| Youn $et\ al.$ [24] (1991) | $^{10}$B$(p, \alpha_0)^7$Be | Fig. 2 (EXFOR)[c] |
| Knape $et\ al.$ [25] (1992) | $^{10}$B$(p, \alpha_0)^7$Be | Fig. 3 |
| Angulo $et\ al.$ [26] (1993) | $^{10}$B$(p, \alpha_0)^7$Be | Table 2 |
| Angulo $et\ al.$ [33] (1993) | $^{10}$B$(p, \alpha_1)^7$Be | Table 1 |
| Chiari $et\ al.$ [55] (2001) | $^{10}$B$(p, p)^{10}$B | EXFOR |
| Spitaleri $et\ al.$ [29] (2014) | $^{10}$B$(p, \alpha_0)^7$Be | Table IV |
| Lombardo $et\ al.$ [52] (2016) | $^{10}$B$(p, \alpha_0)^7$Be | from author |
| this work | $^{10}$B$(p, \alpha_{0,1})^7$Be | |
| **Inconsistent Data** | | |
| Brown $et\ al.$ [30] (1951) | $^{10}$B$(p, \alpha_{0,1})^7$Be | Figs. 9 and 11 (EXFOR) |
| Bach and Livesey [22] (1955) | $^{10}$B$(p, \alpha_0)^7$Be | Table 2 |
| Kalinin $et\ al.$ [42] (1957) | $^{10}$B$(p, \alpha_{\text{total}})^7$Be | Fig. 2 |
| Szabó $et\ al.$ [23] (1972) | $^{10}$B$(p, \alpha_0)^7$Be | Table 1 |
| Caciolli $et\ al.$ [44] (2016) | $^{10}$B$(p, \alpha_{\text{total}})^7$Be | Table 1 |
| **$^7$Be + $\alpha$ Induced Data** | | |
| Freer $et\ al.$ [59] (2012) | $\alpha(^7$Be, $\alpha_{\text{total}})^7$Be and $\alpha(^7$Be, $p_{\text{total}})^{10}$B | Fig. 3 (EXFOR) |
| Yamaguchi $et\ al.$ [60] (2013) | $\alpha(^7$Be, $\alpha_{0,1})^7$Be and $\alpha(^7$Be, $p_{0,1})^{10}$B | Fig. 5 (EXFOR) |

[a] The current analysis suggests a renormalization of this data by a factor of about 2.
[b] Thick target yield unfolded to cross section by Angulo $et\ al.$ [47] (NACRE).
[c] With the correction in the normalization of a factor of 1.83 as suggested by Angulo $et\ al.$ [26].

fitting these data are included but with the addition of the scaling factor as noted in Table I.

One issue in determining the $^{10}$B$(p, \alpha_0)^7$Be cross section is that experiments have focused on different regions, the lack of overlap makes a consistent $R$-matrix analysis more challenging. At lower energies from $140 < E_{\text{lab}} < 300$ keV, the measurement of the $(p, \alpha)$ cross section is handicapped by the large count rate of the scattered protons compared to the rate of the reaction $\alpha$ particles. Below $\approx 140$ keV Angulo $et\ al.$ [26] used degrader foil in front of the charged particle detector to block the high proton flux. The $\alpha$ particles still can penetrate the degrader foil because of their substantially higher energies. At higher energies, above about $E_{\text{lab}} \approx 300$ keV, scattered protons and reaction alphas can be measured simultaneously in a detector. The data of Youn $et\ al.$ [24] are the only ones that bridge this energy gap.

There are significantly fewer measurements of the low energy $^{10}$B$(p, \alpha_1)^7$Be cross section. This is likely because this cross section is between one and three orders of magnitude smaller than the $^{10}$B$(p, \alpha_0)^7$Be cross section below $E_p \approx 1$ MeV. The large gap between the low energy data by Angulo $et\ al.$ [33] and that of Brown $et\ al.$ [30] and Cronin [31], ranging from $160$ keV $< E_{\text{lab}} < 1.3$ MeV,

is bridged by the present data set, showing consistence and good agreement between present and previous data in the overlapping energy ranges.

## C. The Impact of $5/2^+$ Resonance States on the Cross Section Analysis

In the low energy region between the proton separation energy and $E_{c.m.} \approx 1$ MeV, the $S$-factors of $^{10}$B$(p, \alpha_0)^7$Be, $^{10}$B$(p, \alpha_1)^7$Be, and $^{10}$B$(p, \gamma)^{11}$C are similar in shape. Below $E_{c.m.} \approx 1$ MeV, the $S$-factor decreases steadily with energy until at $E_{c.m.} \approx 0.5$ MeV, a region of rapid inflection occurs, with the $S$-factor then rapidly increasing towards lower energies.

This interference pattern is the result of at least two $5/2^+$ states that result in strong resonances in the low energy cross sections. These states are populated by $s$-wave protons and, for the $^{10}$B$(p, \alpha_0)^7$Be reaction, depopulate primarily via $p$-wave $\alpha$ emission to the ground state of $^7$Be. Therefore they are expected, and observed, to have large reduced widths in these channels.

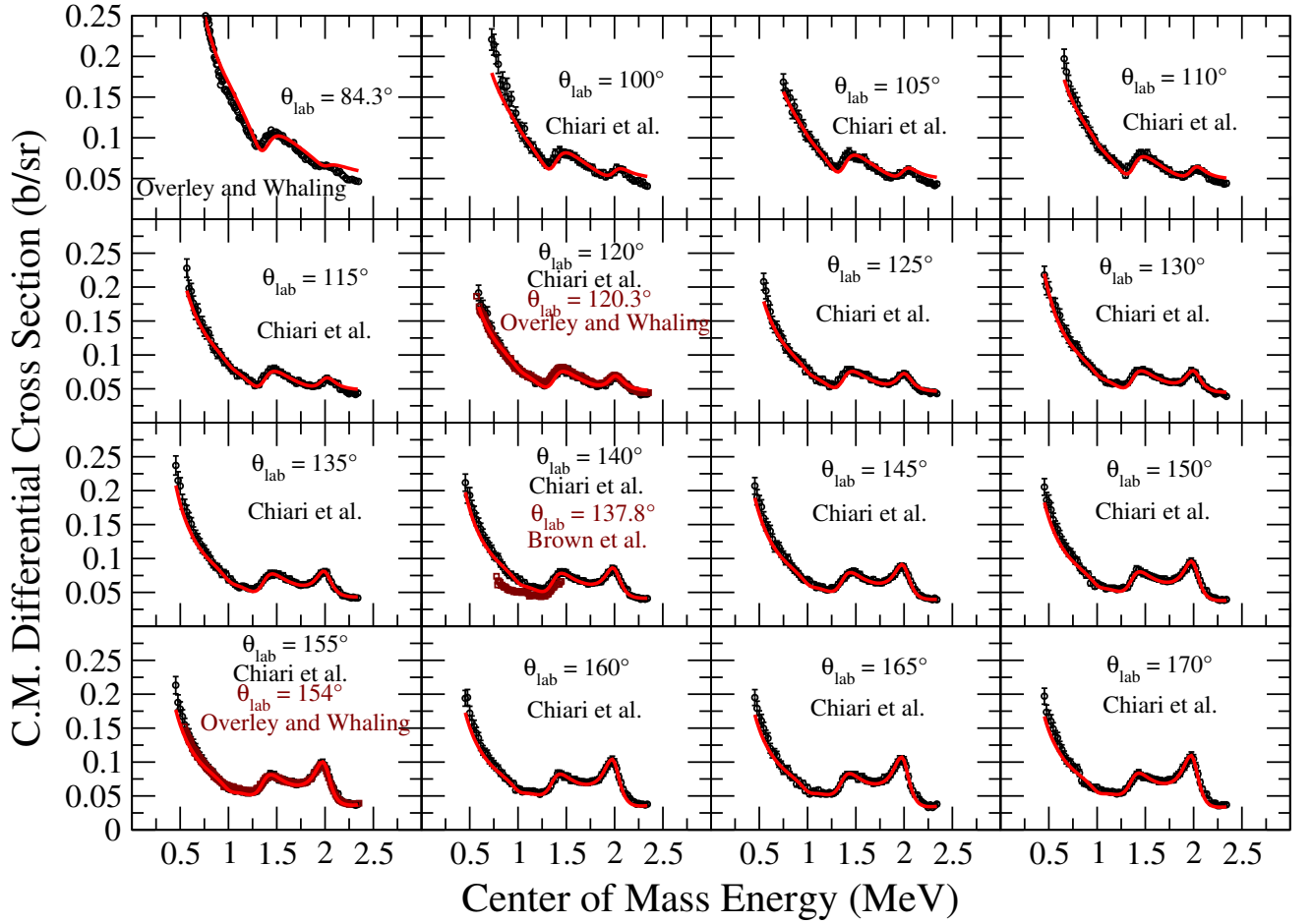The lowest energy of these resonances, corresponding to the level at $E_x = 8.699(2)$ MeV, is just

FIG. 7. (Color online) Comparison of the $^{10}B(p,p)^{10}B$ scattering data taken over a wide angle range by Brown *et al.* [30], Overley and Whaling [61], and Chiari *et al.* [55] with the *R*-matrix fit of this work (solid red line). A good reproduction of the scattering data can be obtained with the levels quoted in the literature. It is of note that in addition to the lowest orbital angular momentum channels possible, the fit requires small but significant angular momentum channels of $l_{min}+2$ in order to achieve a good fit (see Table II).

$E_{c.m.} = 10(2)$ keV above the proton separation energy ($S_p = 8.689$ MeV). This level has been identified in the $^{10}B(^3He,d)^{11}C$ transfer reaction, it's width $\Gamma_{total}$ and spin and parity value $J^\pi$ have also been determined by Fortune *et al.* [62] as $\Gamma_{total} = 15 \pm 1$ keV and $J^\pi = 5/2^+$ respectively. More recently, this state has been measured via the Trojan Horse method by Spitaleri *et al.* [29]. The reduced proton width of this level approaches the single particle limit (see Ref. [50] and references therein), enhancing the low energy cross sections of the $^{10}B(p,\alpha_0)^7Be$, $^{10}B(p,\alpha_1)^7Be$, and $^{10}B(p,\gamma)^{11}C$ reactions. This low energy resonance even effects the scattering cross section, which deviates from Coulomb scattering even at very low energies as discussed in Sec. III A.

To describe the interference at low energy in the capture data, Wiescher *et al.* [50] proposed that another $5/2^+$ level should exist at an excitation energy of $E_x \approx 9.2$ MeV. This resonance is not prominently visible in other reaction channels, but in this analysis it has been found that the inclusion of such a level does result in a significantly better fit in this region. However, it should be stressed that this solution may not be unique and the match between the data and *R*-matrix fit in this region is not yet satisfactory for the $(p,\alpha_0)$ reaction.

At higher energies, Lombardo *et al.* [52] have suggested another $5/2^+$ state at $E_x = 10.10$ MeV. This resonance has also been included in this analysis and has been found to greatly improve the fitting. However, in this analysis the width of this resonance is much larger (see Table II) in order to produce a better fit in the low energy interference region, which was not included in the fit of Lombardo *et al.* [52].

Further, to fit the interference region, the present analysis finds it necessary to include very large background contributions (i.e. large widths for the background poles). This could be neglected in the analysis of Lombardo *et al.* [52] since these background contributions only have a significant effect on the off-resonance interference region that was not previously included. The need for a slowly energy varying background component

(in $S$-factor) has also been noted by Caciolli *et al.* [44]. However, their method of adding a flat constant $S$-factor contribution does not preserve the unitarity of the collision matrix. This breaks one of the very useful constraints of the $R$-matrix approach, conservation of flux.

The very large widths of the background levels suggest another (or several) additional strong resonances at higher energies. Indeed the data of Jenkin *et al.* [32], where measurements were made from $2 < E_{\text{lab}} < 11$ MeV, show many strong, broad, higher energy structures up to $E_{\text{lab}} \approx 8$ MeV. It may therefore be necessary to extend the fitting to higher energy in order to accurately reproduce the interference pattern.

### D. $R$-Matrix Analysis of $^7\text{Be}+\alpha$ Reaction Data

The $R$-matrix analysis of the $^{10}\text{B}+p$ data discussed here should be consistent with $^7\text{Be}+\alpha$ data over a similar excitation energy range since both populate the same $^{11}\text{C}$ compound nucleus. Therefore measurements of $^7\text{Be}(\alpha,\alpha)^7\text{Be}$ reaction could provide key information for resolving the current discrepancies and ambiguities in the $R$-matrix fitting.

There have been recent attempts to investigate the excitation energy range from $E_x = 9$ to $13$ MeV in $^{11}\text{C}$ by measuring the $^7\text{Be}(\alpha,p)^{10}\text{B}$ and $^7\text{Be}(\alpha,\alpha)^7\text{Be}$ reactions in inverse kinematics using thick target techniques by Freer *et al.* [59] and Yamaguchi *et al.* [60]. For these two measurements, the $^7\text{Be}(\alpha,\alpha)^7\text{Be}$ scattering cross sections are in very poor agreement as shown in Fig. 8 of [60]. In addition, Freer *et al.* [59] could not differentiate between $\alpha$ particles arising from elastic and inelastic scattering, both of which are present over much of the energy range. Freer *et al.* [59] assumed that the elastic cross section dominates over the inelastic, but this is not a valid assumption at $E_x > 9.7$ MeV ($E_{\text{c.m.}} > 1.0$ MeV) where the $(p,\alpha_0)$ and $(p,\alpha_1)$ cross sections have shown that the widths of the levels above this energy are close in magnitude (see Fig. 5).

$R$-matrix fits were performed by both Freer *et al.* [59] and Yamaguchi *et al.* [60], but both fit only their data and did not make any comparison calculations with the available proton induced reaction data. Further, the $R$-matrix fit of Freer *et al.* [59] neglected both the inelastic $\alpha$ and proton channels that become significant at higher energies. Both $R$-matrix analyses also neglected the $^8\text{Be} + ^3\text{He}$ channel that also may become significant over the highest energy ranges of their data.

Fig. 8 shows an $R$-matrix calculation for the $^7\text{Be}+\alpha$ and the $^{10}\text{B}+p$ reaction data based on the level parameters given in Freer *et al.* [59] and Yamaguchi *et al.* [60]. In order to achieve a more reasonable comparison, the branching ratios from the literature have been applied to the $\alpha$ widths of Freer *et al.* [59], assuming that these widths represent approximately $\Gamma_{\alpha_0} + \Gamma_{\alpha_1}$. For the $^7\text{Be}+\alpha$ data, only those of Yamaguchi *et al.* [60] are shown as there is some ambiguity in how the data of Freer

*et al.* [59] should be interpreted. Further, additional information about the data of Yamaguchi *et al.* [60] have been given on EXFOR. The $R$-matrix fit reported by Yamaguchi *et al.* [60] (dashed-dotted red line in Fig. 8) can be reasonably reproduced using the level parameters provided in that work. However, when the parameters of Freer *et al.* [59] are used the cross section curve of that work cannot be reproduced. The curve that results from these parameters is given by the dashed red line in Fig. 8. When the level parameters from Freer *et al.* [59] and Yamaguchi *et al.* [60] are then used to calculate the cross sections for the proton induced reactions, the agreement between both the $R$-matrix cross sections and the proton induced data is rather poor for both parameter sets as shown in Fig. 8. This may indicate either a problem with the data or with the understanding of the level structure in this region.

Attempts were made to include the $^7\text{Be}+\alpha$ data in the current $R$-matrix fit, but a consistent fit could not be achieved. For example, Fig. 8 also shows a calculation of the predicted $^7\text{Be}(\alpha,\alpha)^7\text{Be}$ cross section based on the level parameters of this work. Again the agreement is poor. A consistent description of the $^7\text{Be} + \alpha$ and $^{10}\text{B} + p$ data must be achieved before it can be claimed that the level structure in this excitation energy region is well understood. A detailed measurement, likely with a setup that provides a thin target and well defined angles, that covers a wide range in both angle and energy, of the $^7\text{Be}+\alpha$ cross sections is key in achieving this goal. However, so far the very challenging experimental setups that are necessary have prohibited such a measurement.

### IV. DISCUSSION

The present data extends on the results of previous work by closing the gap between the extensive studies in the energy range of astrophysical relevance below 200 keV and the energy range above 1 MeV that has been of interest for the early interpretation of shell structure in light nuclei. In the lower energy range, the $S$-factor data show good agreement with previous work [24, 26, 33]. Fig. 9 shows a subset of the $^{10}\text{B}(p,\alpha_0)^7\text{Be}$ data compilation as well as the data obtained in the present work. An $R$-matrix description of the data was calculated using the resonance parameters listed in the EXFOR 2014 data compilation [17]. While the calculated curve matches the observed low energy increase of the $S$-factor data very well, it fails to reproduce the present data as well as much of the previous data in the $0.5 < E_{\text{c.m.}} < 1.0$. This suggests an additional reaction component in this energy range. This could either be a broad resonance near $E_{\text{c.m.}} = 810$ keV that corresponds to a state at $E_x = 9.5$ MeV excitation energy in the compound nucleus $^{11}\text{C}$ [50] or a direct reaction component [51] as discussed above. Such possibilities were already discussed in the recent paper by Caciolli *et al.* [44]. A much better agreement is reached when using the parameters suggested by
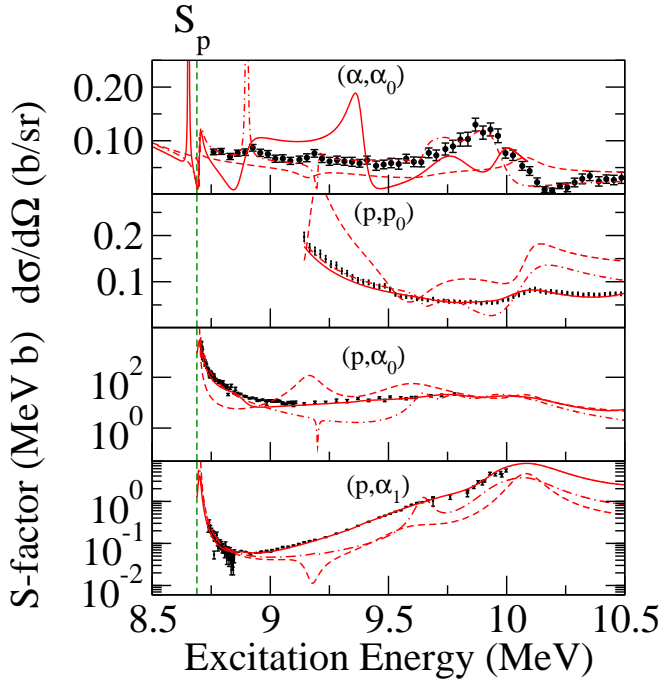
FIG. 8. (Color online) Comparison of $R$-matrix fits to $^7$Be$+\alpha$ data from Yamaguchi *et al.* [60]. The $R$-matrix fit reproduced from the parameters of Freer *et al.* [59] (dashed red line), Yamaguchi *et al.* [60] (dashed-dotted red line), are compared to that produced by the current work (solid red line). Freer *et al.* [59] and Yamaguchi *et al.* [60] fit only the $^7$Be$+\alpha$ data while the current fit includes only $^{10}$B$+p$ data.



FIG. 9. (Color online) Comparison of $R$-matrix fits from the recent publications of Caciolli *et al.* [44] and Lombardo *et al.* [52] as well as a calculation preformed with parameters from the compilation [17]. The wide variation in the fits reflects the complication of achieving a unique fit with the available data.

the $S$-factor data by Lombardo *et al.* [52]. The resulting $R$-matrix description from this work is shown as a solid line in Fig. 9. This fit describes the overall energy dependence of the $S$-factor data by Lombardo *et al.* [52] but fails to provide a satisfying description of the present data set. This again indicates the existence of an additional broad reaction contribution around $E_{c.m.} = 500$ keV.

Figs. 8 and 9 clearly demonstrate the difficulty in describing the $^{11}$C populating cross sections over this energy region. Part of the recent issues have been the use of single reaction fits that ignore the constraints that would be imposed by data in other reaction channels. That said, the authors have attempted such a fit, but have found that there is simply insufficient data, and insufficient consistency among the different data sets, to achieve a unique fit. This is also rather aptly demonstrated by the $R$-matrix parameters given in Table II. While the fit given in this work appears similar to that obtained using the parameters found in the literature, the parameters are quite different. This is mostly the result of the fit's attempt to reproduce the cross section in the vicinity of the interference dip near $E_{c.m.} = 0.5$ MeV.

In order to achieve a more reliable fitting providing a deeper insight into the level structure of $^{11}$C, it is necessary to significantly expand the energy range and provide a consistent set of experimental data ranging from about $E_{c.m.} \approx 250$ keV to 3 MeV. This would allow the fit to
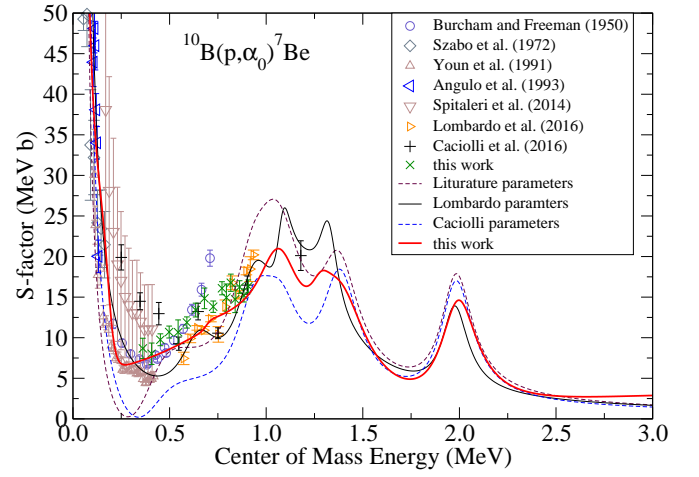
take into account contributions from higher energy resonances in the 1 to 3 MeV proton energy range and it would provide better overlap with the low energy data by Angulo *et al.* [26] and the data range of $^7$Be$+\alpha$ scattering data as provided by Freer *et al.* [59] and Yamaguchi *et al.* [60]. Such a measurement should be made in energy steps fine enough to map all resonances and should be made at several different angles to constrain the spin-parities and interference patterns of the different contributing levels. Further, the measurements should be made for all exit channels, including the $\gamma$ radiative capture channels so that consistent branchings between the different channels can be verified over a broad energy range. Activation measurements should also be made but in conjunction with prompt particle detection measurements so that the discrepancies between these two measurement techniques, which have been observed in the literature previously, can be resolved.

## V. CONCLUSION

In terms of the analysis of the $^{10}$B(p,$\alpha$)$^7$Be reaction as a possible impurity source for aneutronic plasma fusion systems this study confirmed that this reaction only plays a negligible role. Fig. 10 shows the comparison between the $^{11}$B($p, \alpha_1$)$^8$Be and the $^{10}$B(p,$\alpha$)$^7$Be cross sections, which dominate over the energy range of interest. In the critical energy range of aneutronic fusion, in the vicinity of 600 keV, the prime reaction is about fifty times stronger than the background process. Given a natural abundance of 19% for $^{10}$B the rate of the $^{11}$B($p, \alpha_1$)$^8$Be reaction in a natural boron plasma is more than 250 times stronger than the background process. The present study
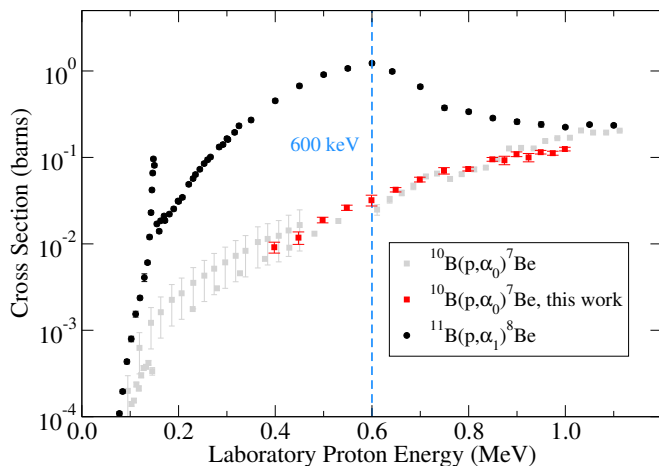
FIG. 10. (Color online) Comparison of the $^{11}$B$(p, \alpha_1)^8$Be reaction data of Becker *et al.* [14] (black circles) with that of the $^{10}$B$(p, \alpha_0)^7$Be reaction from a sampling of previous works [21, 26, 27, 30] (gray squares). The $^{11}$B$(p, \alpha_1)^8$Be and $^{10}$B$(p, \alpha_0)^7$Be are the dominant decay modes for each reaction over the energy range. The present measurements (red squares) are centered on the energy range of interest for aneutronic fusion, which lies in the vicinity of $E_p \approx 600$ keV.

significantly reduced the previous uncertainties associated with this question as outlined in the introduction.

A more concrete prediction is necessary for determining the suitability of the $^{10}$B$(p, \alpha)^7$Be reaction as a signature for laser-driven plasma shots, however, requires a more reliable parametrization over a wider energy range, which has to rely on an $R$-matrix fit over a broad low energy range. The reaction parameters of the here presented $R$-matrix fit are given in Appendix A, Table II. The analysis indicates the need for substantial improvements in the data sets and therefore the present $R$-matrix fit should be viewed as preliminary. To provide a reasonably unique solution and reduce the uncertainty range, additional constraints are necessary.

While the data presented here are a step forward in obtaining added constraint to the $R$-matrix fitting, it is clear that more comprehensive experimental measurements are necessary. In particular, a consistent measurement of all $^{10}$B$+p$ induced reaction channels including radiative capture, expanding on the data of Wiescher *et al.* [50], over a wide energy range and at several angles would lead to a significant improvement in the overall confidence of future $R$-matrix fits by establishing the relative normalizations of the different data sets. The current situation of several patchwork measurements, with sometimes vastly differing normalizations, precludes a confident $R$-matrix analysis. Further, a similar comprehensive measurement of $^7$Be$+\alpha$ reactions over this same excitation energy range would be equally valuable.

## ACKNOWLEDGMENTS

## Appendix A: $R$-matrix fit parameters

The parameters for the preliminary $R$-matrix fit of this work are given in Table II. The level parameters presented in this work should not be viewed as reliable level parameters. They are an example, that can be compared with other analyses that have been used to fit data that populate the $^{11}$C nucleus over a similar energy region, that shows that these solutions are not unique and require further constraint from addition data to achieve a unique solution.

[1] R. Feldbacher and M. Heindler, Nuclear Instruments and Methods in Physics Research Section A: Accelerators, Spectrometers, Detectors and Associated Equipment **271**, 55 (1988).

[2] W. Nevins and R. Swain, Nuclear Fusion **40**, 865 (2000).

[3] R. Kouzes, "PNNL Report 18388," (2009).

[4] D. Shea and D. Morgan, "CRS Report 7-5700, R41419, The Helium-3 Shortage: Supply, Demand, and Options for Congress," (2010).

[5] J. Treglio, Nuclear Instruments and Methods **144**, 65 (1977).

[6] J. Dawson, "Plasma Physics Group Report PPG-273, University of California: CTR using the p-B11 reaction," (1976).

[7] Y. Matsumoto, T. Nagaura, Y. Itoh, S. Oikawa, and T. Watanabe, J. Plasma Fusion Res. SERIES **4**, 422 (2001).

[8] N. Rostoker, M. W. Binderbauer, and H. J. Monkhorst, Science **278**, 1419 (1997).

[9] V. S. Belyaev, A. P. Matafonov, V. I. Vinogradov, V. P. Krainov, V. S. Lisitsa, A. S. Roussetski, G. N. Ignatyev, and V. P. Andrianov, Phys. Rev. E **72**, 026406 (2005).

[10] H. Hora, G. Miley, N. Azizi, B. Malekynia, M. Ghoranneviss, and X. He, Laser and Particle Beams **27**, 491 (2009).

[11] H. Hora, G. Miley, K. Flippo, P. Lalousis, R. Castillo, X. Yang, B. Malekynia, and M. Ghoranneviss, Laser and Particle Beams **29**, 353 (2011).

TABLE II. Energies and particle widths used for the $R$-matrix fit. Parameters marked in **bold** were treated as fit parameters. All others were held constant at their central or nominal values. The $R$-matrix parameterization is that of Brune [63]. Channel radii are $a_{\alpha_0}=a_{\alpha_1}=5.5$ fm and $a_{p_0}=5.0$ fm. Signs on the partial widths indicate the interference signs on the corresponding reduced width amplitudes.

| $J^\pi$ | $E_x$ (MeV) | | particle pair | $(s,l)$ | $\Gamma_i$ (keV) | $\Gamma_\text{total}$ |
| --- | --- | --- | --- | --- | --- | --- |
| | this work | lit. | | this work | | lit. |
| **Physical States** | | | | | | |
| $5/2^+$ | $8.6987^\text{a}$ | 8.699(2) | $p_0$ | $(5/2, 0)$ | $2\times10^{-17}$ | |
| | | | $\alpha_0$ | $(3/2, 1)$ | 15 | |
| | | | $\alpha_1$ | $(1/2, 3)$ | $\mathbf{30\times10^{-3}}$ | |
| | | | total | | 15 | 15(1) |
| $5/2^+$ | **8.88** | 9.2 | $p_0$ | $(5/2, 0)$ | **-0.008** | |
| | | | $p_0$ | $(5/2, 2)$ | **-0.014** | |
| | | | $\alpha_0$ | $(3/2, 1)$ | **105** | |
| | | | $\alpha_1$ | $(1/2, 3)$ | **-0.005** | |
| | | | total | | 105 | 500(90) |
| $(5/2^-)$ | 9.38 | $9.38^\text{b}$ | $p_0$ | $(7/2, 1)$ | **0.274** | |
| | | | $\alpha_0$ | $(3/2, 2)$ | **81** | |
| | | | $\alpha_1$ | $(1/2, 2)$ | **0.016** | |
| | | | total | | 81 | $239^\text{b}$ |
| $(3/2^-)$ | $9.65^\text{b}$ | 9.645(50) | $p_0$ | $(5/2, 1)$ | **-0.94** | |
| | | | $\alpha_0$ | $(3/2, 0)$ | **3.4** | |
| | | | $\alpha_1$ | $(1/2, 2)$ | **388** | |
| | | | total | | 388 | 210(40) |
| $(5/2^-)$ | 9.80 | 9.80(5) | $p_0$ | $(5/2, 1)$ | **-33** | |
| | | | $p_0$ | $(7/2, 1)$ | **2.1** | |
| | | | $\alpha_0$ | $(3/2, 2)$ | **250** | |
| | | | $\alpha_1$ | $(1/2, 2)$ | **10** | |
| | | | total | | 295 | 240(50) |
| $(7/2^-)$ | 9.98 | 9.97(5) | $p_0$ | $(5/2, 1)$ | **-2.9** | |
| | | | $p_0$ | $(7/2, 1)$ | **-5.8** | |
| | | | $\alpha_0$ | $(3/2, 2)$ | **98** | |
| | | | $\alpha_1$ | $(1/2, 4)$ | **42** | |
| | | | total | | 149 | 120(20) |
| $7/2^+$ | **10.125** | 10.038(5) | $p_0$ | $(5/2, 0)$ | **-52** | |
| | | | $p_0$ | $(5/2, 2)$ | **55** | |
| | | | $p_0$ | $(7/2, 2)$ | **49** | |
| | | | $\alpha_0$ | $(3/2, 1)$ | **110** | |
| | | | $\alpha_1$ | $(1/2, 3)$ | **-105** | |
| | | | total | | 371 | $\approx230$ |
| $(5/2^+)$ | 10.15 | $10.15^\text{b}$ | $p_0$ | $(5/2, 0)$ | **-49** | |
| | | | $p_0$ | $(5/2, 2)$ | **12** | |
| | | | $p_0$ | $(7/2, 2)$ | **-4.8** | |
| | | | $\alpha_0$ | $(3/2, 1)$ | $\mathbf{2.32\times10^3}$ | |
| | | | $\alpha_1$ | $(1/2, 3)$ | **31.4** | |
| | | | total | | $2.37\times10^3$ | $183^\text{a}$ |
| $9/2^+$ | **10.694** | 10.679(5) | $p_0$ | $(5/2, 2)$ | **1.8** | |
| | | | $p_0$ | $(7/2, 2)$ | **-97** | |
| | | | $\alpha_0$ | $(3/2, 3)$ | **125** | |
| | | | $\alpha_1$ | $(1/2, 5)$ | **11** | |
| | | | total | | 235 | 200(30) |
| **Background Poles** | | | | | | |
| $5/2^-$ | 15 | | $p_0$ | $(5/2, 1)$ | $\mathbf{4.3\times10^3}$ | |
| | | | $\alpha_0$ | $(3/2, 2)$ | $\mathbf{-9.1\times10^3}$ | |
| | | | $\alpha_1$ | $(1/2, 2)$ | $\mathbf{-7.1\times10^3}$ | |
| $5/2^+$ | 15 | | $p_0$ | $(5/2, 0)$ | $\mathbf{-50\times10^3}$ | |
| | | | $\alpha_0$ | $(3/2, 1)$ | $\mathbf{81\times10^3}$ | |
| | | | $\alpha_1$ | $(1/2, 3)$ | $\mathbf{26\times10^3}$ | |

[a] Energy fixed at that of Spitaleri *et al.* [29].
[b] From Lombardo *et al.* [52].

[12] I. Last, S. Ron, and J. Jortner, Phys. Rev. A **83**, 043202 (2011).

[13] J. J. Chapman, *2011 Abstracts IEEE International Conference on Plasma Science*, , 1 (2011).

[14] H. W. Becker, C. Rolfs, and H. P. Trautvetter, Zeitschrift für Physik A Atomic Nuclei **327**, 341 (1987).

[15] V. S. Belyaev, V. I. Vinogradov, A. P. Matafonov, S. M. Rybakov, V. P. Krainov, V. S. Lisitsa, V. P. Andrianov, G. N. Ignatiev, V. S. Bushuev, A. I. Gromov, A. S. Rusetsky, and V. A. Dravin, Physics of Atomic Nuclei **72**, 1077 (2009).

[16] C. N. Davids, A. J. Elwyn, B. W. Filippone, S. B. Kaufman, K. E. Rehm, and J. P. Schiffer, Phys. Rev. C **28**, 885 (1983).

[17] N. Otuka, E. Dupont, V. Semkova, B. Pritychenko, A. Blokhin, M. Aikawa, S. Babykina, M. Bossant, G. Chen, S. Dunaeva, R. Forrest, T. Fukahori, N. Furutachi, S. Ganesan, Z. Ge, O. Gritzay, M. Herman, S. Hlava, K. Kat, B. Lalremruata, Y. Lee, A. Makinaga, K. Matsumoto, M. Mikhaylyukova, G. Pikulina, V. Pronyaev, A. Saxena, O. Schwerer, S. Simakov, N. Soppera, R. Suzuki, S. Takcs, X. Tao, S. Taova, F. Trknyi, V. Varlamov, J. Wang, S. Yang, V. Zerkin, and Y. Zhuang, Nuclear Data Sheets **120**, 272 (2014).

[18] National Ignition Facility, https://lasers.llnl.gov/.

[19] R. Hatarik, D. B. Sayre, J. A. Caggiano, T. Phillips, M. J. Eckart, E. J. Bond, C. Cerjan, G. P. Grim, E. P. Hartouni, J. P. Knauer, J. M. Mcnaney, and D. H. Munro, Journal of Applied Physics **118**, 184502 (2015).

[20] W. Burcham and J. M. Freeman, The London, Edinburgh, and Dublin Philosophical Magazine and Journal of Science **40**, 807 (1949), http://dx.doi.org/10.1080/14786444908561405.

[21] W. Burcham and J. M. Freeman, The London, Edinburgh, and Dublin Philosophical Magazine and Journal of Science **41**, 337 (1950), http://dx.doi.org/10.1080/14786445008560970.

[22] G. Bach and D. Livesey, The London, Edinburgh, and Dublin Philosophical Magazine and Journal of Science **46**, 824 (1955), http://dx.doi.org/10.1080/14786440808561234.

[23] J. Szabó, J. Csikai, and M. Várnagy, Nuclear Physics A **195**, 527 (1972).

[24] M. Youn, H. Chung, J. Kim, H. Bhang, and K.-H. Chung, Nuclear Physics A **533**, 321 (1991).

[25] F. Knape, H. Bucka, and P. Heide, in *Nuclei in the Cosmos 2*, edited by F. Kaeppeler and K. Wisshak (1993) pp. 175–180.

[26] C. Angulo, S. Engstler, G. Raimann, C. Rolfs, W. H. Schulte, and E. Somorjai, Zeitschrift für Physik A Hadrons and Nuclei **345**, 231 (1993).

[27] L. Lamia, S. Romano, N. Carlin, S. Cherubini, V. Crucill, M. D. Moura, M. D. Santo, M. Munhoz, M. Gulino, R. L. Neto, M. L. Cognata, F. Mud, R. Pizzone, S. Puglia, M. Sergi, F. Souza, C. Spitaleri, A. Suaide, E. Szanto, A. S. de Toledo, S. Tudisco, and A. Tumino, Nuclear Physics A **787**, 309 (2007).

[28] L. Lamia, S. Puglia, C. Spitaleri, S. Romano, M. G. D. Santo, N. Carlin, M. G. Munhoz, S. Cherubini, G. Kiss, V. Kroha, S. Kubono, M. L. Cognata, C.-B. Li, R. Pizzone, Q.-G. Wen, M. Sergi, A. S. de Toledo, Y. Wakabayashi, H. Yamaguchi, and S.-H. Zhou, Nuclear Physics A **834**, 655c (2010).

[29] C. Spitaleri, L. Lamia, S. M. R. Puglia, S. Romano, M. La Cognata, V. Crucillà, R. G. Pizzone, G. G. Rapisarda, M. L. Sergi, M. G. Del Santo, N. Carlin, M. G. Munhoz, F. A. Souza, A. Szanto de Toledo, A. Tumino, B. Irgaziev, A. Mukhamedzhanov, G. Tabacaru, V. Burjan, V. Kroha, Z. Hons, J. Mrazek, S.-H. Zhou, C. Li, Q. Wen, Y. Wakabayashi, H. Yamaguchi, and E. Somorjai, Phys. Rev. C **90**, 035801 (2014).

[30] A. B. Brown, C. W. Snyder, W. A. Fowler, and C. C. Lauritsen, Phys. Rev. **82**, 159 (1951).

[31] J. W. Cronin, Phys. Rev. **101**, 298 (1956).

[32] J. Jenkin, L. Earwaker, and E. Titterton, Nuclear Physics **50**, 516 (1964).

[33] C. Angulo, W. H. Schulte, D. Zahnow, G. Raimann, and C. Rolfs, Zeitschrift für Physik A Hadrons and Nuclei **345**, 333 (1993).

[34] R. B. Day and T. Huus, Phys. Rev. **95**, 1003 (1954).

[35] S. E. Hunt, R. A. Pope, and W. W. Evans, Phys. Rev. **106**, 1012 (1957).

[36] T. Ophel, R. Glover, and E. Titterton, Nuclear Physics **33**, 198 (1962).

[37] E. Bernstein, Nuclear Physics **59**, 525 (1964).

[38] R. E. Segel, P. P. Singh, S. S. Hanna, and M. A. Grace, Phys. Rev. **145**, 736 (1966).

[39] Y. Rihet, G. Costa, C. Gerardin, and R. Seltz, Phys. Rev. C **20**, 1583 (1979).

[40] C. Boni, E. Cereda, G. Marcazzan, and V. D. Tomasi, Nuclear Instruments and Methods in Physics Research Section B: Beam Interactions with Materials and Atoms **35**, 80 (1988).

[41] A. Lagoyannis, K. Preketes-Sigalas, M. Axiotis, V. Foteinou, S. Harissopulos, M. Kokkoris, P. Misaelides, V. Paneta, and N. Patronis, Nuclear Instruments and Methods in Physics Research Section B: Beam Interactions with Materials and Atoms **342**, 271 (2015).

[42] S. P. Kalinin, A. A. Ogloblin, and Y. M. Petrov, The Soviet Journal of Atomic Energy **2**, 193 (1957).

[43] N. Roughton, M. Fritts, R. Peterson, C. Zaidins, and C. Hansen, Atomic Data and Nuclear Data Tables **23**, 177 (1979).

[44] A. Caciolli, R. Depalo, C. Broggini, M. La Cognata, L. Lamia, R. Menegazzo, L. Mou, S. M. R. Puglia, V. Rigato, S. Romano, C. Rossi Alvarez, M. L. Sergi, C. Spitaleri, and A. Tumino, The European Physical Journal A **52**, 1 (2016).

[45] A. Kafkarkou, M. Ahmed, P. Chu, R. France, H. Karwowski, D. Kendellen, G. Laskaris, I. Mazumdar, J. Mueller, L. Myers, R. Prior, M. Sikora, M. Spraker, H. Weller, and W. Zimmerman, Nuclear Instruments and Methods in Physics Research Section B: Beam Interactions with Materials and Atoms **316**, 48 (2013).

[46] J. Kelley, E. Kwan, J. Purcell, C. Sheu, and H. Weller, Nuclear Physics A **880**, 88 (2012).

[47] C. Angulo, M. Arnould, M. Rayet, P. Descouvemont, D. Baye, C. Leclercq-Willain, A. Coc, S. Barhoumi, P. Aguer, C. Rolfs, R. Kunz, J. Hammer, A. Mayer, T. Paradellis, S. Kossionides, C. Chronidou, K. Spyrou, S. Degl'Innocenti, G. Fiorentini, B. Ricci, S. Zavatarelli, C. Providencia, H. Wolters, J. Soares, C. Grama, J. Rahighi, A. Shotter, and M. L. Rachti, Nuclear Physics A **656**, 3 (1999).

[48] L. Lamia, C. Spitaleri, N. Carlin, S. Cherubini, M. G. D. Szanto, M. Gulino, M. L. Cognata, M. G. Munhoz, R. G. Pizzone, S. M. R. Puglia, G. G. Rapisarda, S. Romano, M. L. Sergi, A. S. de Toledo, S. Tudisco, and A. Tumino, IL NUOVO CIMENTO B **31** (2009), 10.1393/ncc/i2009-10303-2.

[49] C. Spitaleri, S. M. R. Puglia, M. La Cognata, L. Lamia, S. Cherubini, A. Cvetinović, G. D'Agata, M. Gulino, G. L. Guardo, I. Indelicato, R. G. Pizzone, G. G. Rapisarda, S. Romano, M. L. Sergi, R. Spartá, S. Tudisco, A. Tumino, M. G. Del Santo, N. Carlin, M. G. Munhoz, F. A. Souza, A. S. de Toledo, A. Mukhamedzhanov, C. Broggini, A. Caciolli, R. Depalo, R. Menegazzo, V. Rigato, I. Lombardo, and D. Dell'Aquila, Phys. Rev. C **95**, 035801 (2017).

[50] M. Wiescher, R. N. Boyd, S. L. Blatt, L. J. Rybarcyk, J. A. Spizuoco, R. E. Azuma, E. T. H. Clifford, J. D. King, J. Görres, C. Rolfs, and A. Vlieks, Phys. Rev. C **28**, 1431 (1983).

[51] T. Rauscher and G. Raimann, Phys. Rev. C **53**, 2496 (1996).

[52] I. Lombardo, D. Dell'Aquila, F. Conte, L. Francalanza, M. L. Cognata, L. Lamia, R. L. Torre, G. Spadaccini, C. Spitaleri, and M. Vigilante, Journal of Physics G: Nuclear and Particle Physics **43**, 045109 (2016).

[53] J. Jenkin, L. Earwaker, and E. Titterton, Physics Letters **4**, 142 (1963).

[54] R. Zehringer, H. Knzli, P. Oelhafen, and C. Hollenstein, Journal of Nuclear Materials **176177**, 370 (1990).

[55] M. Chiari, L. Giuntini, P. Mand, and N. Taccetti, Nuclear Instruments and Methods in Physics Research Section B: Beam Interactions with Materials and Atoms **184**, 309 (2001).

[56] H. Gove, *Nuclear Reactions*, edited by P. Endt and M. Demeur, Vol. 1 (North-Holland: Amsterdam, 1959).

[57] R. Morlock, R. Kunz, A. Mayer, M. Jaeger, A. Müller, J. W. Hammer, P. Mohr, H. Oberhummer, G. Staudt, and V. Kölle, Phys. Rev. Lett. **79**, 3837 (1997).

[58] B. Paine and D. Sargood, Nuclear Physics A **331**, 389 (1979).

[59] M. Freer, N. L. Achouri, C. Angulo, N. I. Ashwood, D. W. Bardayan, S. Brown, W. N. Catford, K. A. Chipps, N. Curtis, P. Demaret, C. Harlin, B. Laurent, J. D. Malcolm, M. Milin, T. Munoz-Britton, N. A. Orr, S. D. Pain, D. Price, R. Raabe, N. Soić, J. S. Thomas, C. Wheldon, G. Wilson, and V. A. Ziman, Phys. Rev. C **85**, 014304 (2012).

[60] H. Yamaguchi, D. Kahl, Y. Wakabayashi, S. Kubono, T. Hashimoto, S. Hayakawa, T. Kawabata, N. Iwasa, T. Teranishi, Y. K. Kwon, D. N. Binh, L. H. Khiem, and N. N. Duy, Phys. Rev. C **87**, 034303 (2013).

[61] J. C. Overley and W. Whaling, Phys. Rev. **128**, 315 (1962).

[62] H. T. Fortune, H. G. Bingham, J. D. Garrett, and R. Middleton, Phys. Rev. C **7**, 136 (1973).

[63] C. R. Brune, Phys. Rev. C **66**, 044611 (2002).